

Nonadiabatic Born effective charges in metals and the Drude weight

Cyrus E. Dreyer,^{1,2} Sinisa Coh,³ and Massimiliano Stengel^{4,5}

¹*Department of Physics and Astronomy, Stony Brook University, Stony Brook, New York, 11794-3800, USA*

²*Center for Computational Quantum Physics, Flatiron Institute,
162 5th Avenue, New York, New York 10010, USA*

³*Materials Science and Mechanical Engineering, University of California Riverside, CA 92521, USA*

⁴*Institut de Ciència de Materials de Barcelona (ICMAB-CSIC), Campus UAB, 08193 Bellaterra, Spain*

⁵*ICREA-Institució Catalana de Recerca i Estudis Avançats, 08010 Barcelona, Spain*

(Dated: December 23, 2024)

In insulators, Born effective charges describe the electrical polarization induced by the displacement of individual atomic sublattices. Such a physical property is at first sight irrelevant for metals and doped semiconductors, where the macroscopic polarization is ill-defined. Here we show that, in clean conductors, going beyond the adiabatic approximation results in nonadiabatic Born effective charges that are well defined in the low-frequency limit. In addition, we find that the sublattice sum of the nonadiabatic Born effective charges does not vanish as it does in the insulating case, but instead is proportional to the Drude weight. We demonstrate these formal results with density functional perturbation theory calculations of Al, and electron-doped SnS₂ and SrTiO₃.

Lattice vibrations and electron-phonon coupling play a crucial role in the thermodynamic and transport properties of crystals [1]; *ab-initio* linear-response calculations based on density-functional perturbation theory [2] (DFPT) have long been established as a powerful tool for their quantitative understanding. Two key quantities involved are the zone-center dynamical matrix, defined as the second derivative of the total energy with respect to atomic displacements, and the “Born effective” dynamical charges (BECs) for the ions [3–5], defined as the polarization induced by an atomic displacement. Accurate knowledge of the BECs is important for understanding the interplay between electric fields and long-wavelength optical phonons [3, 6–9], the lattice contribution to dielectric screening [3, 6] and electromechanical coupling [10–12], and the polar properties of ferroelectrics [13–15].

The conceptual foundation of *ab-initio* lattice dynamics rests on the seminal work by Pick, Cohen and Martin (PCM) [5], where the separation between the long-range and short-range interatomic forces, together with the acoustic sum rule (ASR), were formally established in the framework of fundamental electronic-structure theory. The ASR states that a rigid translation of the crystal lattice does not produce either forces on the individual atoms, or a net electrical polarization, and can be regarded as a consequence of the overall translational invariance and charge neutrality. As a result of the ASR, the sublattice sums of both the zone-center force-constants and the BECs vanish.

In metals, at first sight, only the force-constant ASR appears to be relevant since the polarization is ill-defined [16]. A hypothetical definition of the BECs as the dipolar moment of the first-order charge induced by an atomic displacement would also be problematic, since the free carriers screen any long-range electrostatic perturbation. However, complete screening only occurs within the adiabatic (or Born-Oppenheimer [17]) approximation, a

key assumption in the PCM derivations. The adiabatic approximation is usually justified in insulators, where the electronic gap is much larger than typical optical phonon frequencies (of the order of < 200 meV for inorganic materials [18]), but generally breaks down in a metallic or doped semiconducting systems. Manifestation of nonadiabaticity in lattice dynamics are well known, e.g., plasmon-phonon coupling [19, 20] and renormalization of the phonon frequencies [21]. In particular, there exists a region near the zone center where the phase velocity of an optical phonon is large compared to the Fermi velocity [22]. In such a regime, the nonadiabatic dynamical matrix may significantly differ from its adiabatic counterpart. Also, free carriers are unable to screen the long-range electric fields, and signatures of the BECs can be detected experimentally as resonances in the reflectivity spectra [23, 24] or shifts in the plasmon frequency [19].

Given the rapidly growing interest in the aforementioned class of phenomena [1, 21, 22, 24, 25], it is becoming increasingly urgent to firm up the fundamental theory of nonadiabatic response functions, whose properties and phenomenology may significantly depart from the corresponding adiabatic quantities in insulators. In particular, it would be desirable to understand the physical origin of the ASR breakdown that was pointed out in Ref. [24]. Also, the recent surge of interest in “ferroelectric metals” [26, 27] has provided additional motivation to understand BECs in metallic systems.

Here we show that, in the low-frequency regime relevant for lattice dynamics, the nonadiabatic BECs (naBECs) are well-defined real quantities, as long as time-reversal symmetry is preserved. Remarkably, we find that their sublattice sum in general does not vanish but tends to the *Drude weight* (DW), which gives the density of free electrons available for conduction. This generalized sum rule implies that the naBECs never vanish in metals or doped semiconductors (not even in ele-

mental quasi-free-electron crystals), with important implications for the coupled lattice and carrier dynamics near the zone center. This result also clarifies the interpretation of the DW as a measure of the inertia of the conduction electrons, which the underlying lattice potential cannot drag along if subjected to a sufficiently rapid oscillation. We demonstrate these above formal results by performing calculations in the framework of DFPT for a prototypical metal (Al) and two doped semiconductors (SnS₂ and SrTiO₃). In the latter, we find that naBECs can deviate significantly from their values in the undoped material.

We shall frame our discussion in terms of generalized susceptibility functions, $\chi_{\lambda_1\lambda_2}(\omega, \mathbf{q})$, describing the λ_1 -response to the perturbation λ_2 , modulated by a wavevector \mathbf{q} and at a frequency ω . We focus henceforth on the cases where $\lambda_{1,2}$ are either an atomic displacement of sublattice κ in direction α ($\tau_{\kappa\alpha}$) or a component of the vector potential (A_α). The purely electromagnetic case is well known: $\chi_{A_\alpha A_\beta}(\omega, \mathbf{q})$ is the current-current response [28], whose long-wavelength limit relates to the macroscopic optical conductivity via [29]

$$\sigma_{\alpha\beta}(\omega) = \frac{i}{\omega} \lim_{\mathbf{q} \rightarrow 0} \chi_{A_\alpha A_\beta}(\omega, \mathbf{q}). \quad (1)$$

(As customary, we shall assume that the frequency has a small imaginary part, $i\eta$, to ensure causality [30].) In close analogy with Eq. (1), we shall define naBECs as [23, 24]

$$Z_{\kappa\beta}^{(\alpha)}(\omega) = -\frac{i}{\omega} \lim_{\mathbf{q} \rightarrow 0} \chi_{A_\alpha \tau_{\kappa\beta}}(\omega, \mathbf{q}). \quad (2)$$

Note that the replacement of one of the two perturbations with an atomic displacement, $\tau_{\kappa\beta}$, endows Eq. (2) with the physical meaning of a current response to the atomic *velocity*. The negative sign compared to Eq. (1) reflects the fact that the time derivative of the vector potential is *minus* the electric field, $\mathbf{E} = -\partial_t \mathbf{A}$.

For most materials, the interesting physics is contained in the small- ω behavior of $Z_{\kappa\beta}^{(\alpha)}(\omega)$, i.e., at the frequencies that are relevant for lattice dynamics. Within such a regime, the conductivity [Eq. (1)] vanishes in trivial insulators [30] (it can acquire a quantized antisymmetric contribution in Chern insulators [31]), and Eq. (2) reduces to the standard linear-response formula [2, 6, 32] for the *adiabatic* BEC. Note that, in the insulating case, the result is also independent of the order of the long-wavelength and small-frequency limits.

In metals, Eq. (1) diverges as $\omega \rightarrow 0$, resulting in the Drude peak in the longitudinal conductivity [29]. Since Eq. (2) is formally similar to Eq. (1), it is reasonable to wonder whether $Z_{\kappa\beta}^{(\alpha)}(\omega \rightarrow 0)$ diverges as well, or tends to a finite constant. The answer to this crucial question can be deduced by a simple analysis of Eq. (2) and Eq. (1). The divergence in $\sigma_{\alpha\beta}(\omega \rightarrow 0)$ is rooted in the fact that

$\chi_{A_\alpha A_\beta}$ tends to a finite nonzero limit in all metals,

$$\lim_{\omega \rightarrow 0} \chi_{A_\alpha A_\beta}(\omega) = \frac{D_{\alpha\beta}}{\pi}, \quad (3)$$

where $D_{\alpha\beta}$ is the Drude weight (DW) tensor [30]. The situation regarding the mixed response to a vector potential and an atomic displacement clearly differs, as it requires time-reversal (TR) symmetry to be broken in order to be nonzero. (\mathbf{A} is odd with respect to both TR and space inversion, while τ_κ is TR-even.) This simple argument guarantees that in TR-symmetric metals, where a steady current in response to a static atomic displacement is forbidden, $\chi_{A_\alpha \tau_{\kappa\beta}}(\omega \rightarrow 0)$ vanishes and therefore $Z_{\kappa\beta}^{(\alpha)}(\omega \rightarrow 0)$ is well defined. Note that, unlike the insulating case, here the order of the $\mathbf{q} \rightarrow 0$ and $\omega \rightarrow 0$ limits do not commute; our prescription of taking the $\mathbf{q} \rightarrow 0$ first is relevant for optical phonons, which retain a finite frequency in the long-wavelength limit.

Acoustic phonons are, in principle, not concerned by our arguments, since their frequency vanishes linearly with momentum in a neighborhood of the zone center. Yet, in the following we shall consider hypothetical long-wavelength acoustic phonons whose limiting $\mathbf{q} \rightarrow 0$ frequency is artificially assumed to remain finite. This assumption, while physically unrealistic, will serve as an intermediate step towards the derivation of a sum rule for the nonadiabatic BECs, which shall be our next goal. The rationale behind this procedure is that an acoustic phonon at $\mathbf{q}=0$ reduces to a rigid translation of the whole crystal lattice. In the linear regime, a translation can be regarded as the sum of the displacements of all individual atomic sublattices; thus, by looking at the current density induced by a “zone-center acoustic phonon” that is externally modulated in time at a frequency ω , one can directly infer the sublattice sum of the naBECs [Eq. (2)].

The advantage of such an approach is that the acoustic phonon perturbation enjoys a remarkably compact expression when rewritten, via a coordinate transformation, in the curvilinear frame that is co-moving with the atoms [33–35]. Thereby, an acoustic phonon can be recast as a “static” strain contribution that only depends on the metric of the deformation, plus a “dynamical” effective vector potential that results from the inertia of the electrons upon local displacements of the coordinate frame [34]. In a Kohn-Sham [36] density-functional context (see supplemental material (SM) [37] Sec. S1), we can then write the sublattice sum of the first-order phonon ($\tau_{\kappa\beta}$) Hamiltonians as [34]

$$\sum_{\kappa} \hat{\mathcal{H}}^{\tau_{\kappa\beta}}(\omega, \mathbf{q}) = \hat{\mathcal{H}}^{(\beta)}(\omega, \mathbf{q}) + i\omega \hat{\mathcal{H}}^{A_\beta}(\omega, \mathbf{q}), \quad (4)$$

where $\hat{\mathcal{H}}^{(\beta)}(\omega, \mathbf{q})$ is the “metric wave” Hamiltonian of Refs. 34 and 35, and $\hat{\mathcal{H}}^{A_\beta}(\omega, \mathbf{q})$ is the additional effective vector potential perturbation.

As a result of translational invariance, $\hat{\mathcal{H}}^{(\beta)}(\omega, \mathbf{q})$ identically vanishes at the zone center [35], and thus the rigid displacement of the lattice reduces to the vector-potential perturbation term at $\mathbf{q} = 0$. By combining this observation with Eqs. (1) and (2), we readily arrive at

$$\frac{1}{\Omega} \sum_{\kappa} Z_{\kappa\beta}^{(\alpha)}(\omega) = i\omega\sigma_{\alpha\beta}(\omega), \quad (5)$$

relating the sum of the naBECs to the optical conductivity (Ω is the cell volume). From Eq. (3) we find that the small-frequency limit of Eq. (5) becomes,

$$\frac{1}{\Omega} \sum_{\kappa} Z_{\alpha,\kappa\beta}^* = \frac{D_{\alpha\beta}}{\pi}, \quad (6)$$

where $Z_{\alpha,\kappa\beta}^* \equiv Z_{\kappa\beta}^{(\alpha)}(\omega \rightarrow 0)$ is the zero-frequency limit of the naBEC. We call Eq. (6) the *naBEC sum rule for metals* and, along with Eq. (5), is the central result of this work. Of course, in an insulator $D_{\alpha\beta}$ vanishes, and we recover the well-known version of the acoustic sum rule [5], $\sum_{\kappa} Z_{\alpha,\kappa\beta}^* = 0$. The physical interpretation of Eq. (6) is that the DW can be thought of as quantifying the portion of the electron charge that is “free,” i.e., not bound to the underlying atomic lattice. When the crystal is rigidly translated, going beyond the adiabatic assumption means that exactly this charge is “left behind,” resulting in a positive current due to the displacement of the uncompensated nuclear charges. This provides an alternative physical interpretation of the DW, which is based on lattice dynamics rather than electronic transport.

The above results are relevant for the clean limit of a metal or semiconductor, i.e., we assume an optical phonon of frequency ω that is much larger than the inverse carrier lifetime, $1/\tau$ [21, 22]. Thus, the limit $Z_{\kappa\beta}^{(\alpha)}(\omega \rightarrow 0)$ in Eq. (6) should not be taken literally: the result only holds for a window of frequencies where $\omega \gg 1/\tau$, and both parameters are far smaller than interband resonances. Whenever the clean condition breaks down, we expect the naBECs to vanish as the carriers have enough time to relax to the instantaneous electronic ground state along the phonon displacement coordinate. This is consistent with the arguments of Refs. 38, 21, and 22, made for nonadiabatic corrections to the phonon frequencies. Interestingly, Eq. (5) appears to be qualitatively correct even in presence of dissipation – the DC limit of the conductivity is finite, which implies that the ASR is recovered for $\omega \rightarrow 0$. Deriving the nonadiabatic current in the co-moving reference frame was key to achieving the qualitatively correct results, as it reflects the intuitive idea that scattering events tend to equilibrate the average momentum of the carriers with respect to the underlying crystal lattice, rather than the laboratory frame [39].

We will now demonstrate the sum rule in Eq. (6) with DFPT calculations performed on three systems, the face-centered cubic (FCC) phase of Al, electron-doped bulk ($P\bar{3}m1$) SnS_2 and electron-doped cubic ($Pm\bar{3}m$) SrTiO_3 (STO). The details of the implementation, computational parameters, and numerical convergence for these calculations are given in the SM [37] Secs. S1 D and S2.

We calculate the naBECs in the $\omega \rightarrow 0$ limit as (see [37], Sec. S1 and Refs. [23, 24])

$$Z_{\alpha,\kappa\beta}^* = Z_{\kappa}^{\text{ion}}\delta_{\alpha\beta} - \text{Im} \lim_{\eta \rightarrow 0^+} \int [d^3k] \sum_{n \neq m} \frac{f_{n\mathbf{k}} - f_{m\mathbf{k}}}{(\epsilon_{n\mathbf{k}} - \epsilon_{m\mathbf{k}})(\epsilon_{n\mathbf{k}} - \epsilon_{m\mathbf{k}} + i\eta)} \langle u_{n\mathbf{k}} | \hat{H}_{\mathbf{k}}^{A\alpha} | u_{m\mathbf{k}} \rangle \langle u_{m\mathbf{k}} | \hat{\mathcal{H}}_{\mathbf{k}}^{\tau_{\kappa\beta}} | u_{n\mathbf{k}} \rangle, \quad (7)$$

where Z_{κ}^{ion} is the ionic (i.e., pseudopotential) charge, $\epsilon_{n\mathbf{k}}$ and $f_{n\mathbf{k}} = f(\epsilon_{n\mathbf{k}})$ are the energy and Fermi occupation factor of band n and k -point \mathbf{k} , $u_{n\mathbf{k}}$ is the cell-periodic part of the corresponding Bloch function, $\hat{H}_{\mathbf{k}}^{A\alpha}$ is the \mathbf{k} -derivative of the Hamiltonian, and $\hat{\mathcal{H}}_{\mathbf{k}}^{\tau_{\kappa\beta}}$ is the screened (i.e., including self-consistent fields) first-order phonon Hamiltonian. The DW, in turn, is calculated via [30]

$$\frac{\Omega}{\pi} D_{\alpha\beta} = - \int [d^3k] \sum_n \frac{\partial f(\epsilon_{n\mathbf{k}})}{\partial \epsilon} v_{n\mathbf{k}}^{(\alpha)} v_{n\mathbf{k}}^{(\beta)}, \quad (8)$$

where $v_{n\mathbf{k}}^{(\alpha)} = \langle u_{n\mathbf{k}} | \hat{H}_{\mathbf{k}}^{A\alpha} | u_{n\mathbf{k}} \rangle$ is the α component of the band velocity. Note that, because of a technical subtlety related to the use of nonlocal pseudopotentials (nlPSP) in the calculations, the sum rule of Eq. (6) is exactly satisfied only if the second band velocity in Eq. (8) is replaced

with the canonical momentum, $\tilde{v}_{n\mathbf{k}}^{(\beta)} = \langle u_{n\mathbf{k}} | \hat{p}_{\beta\mathbf{k}} | u_{n\mathbf{k}} \rangle$. [We shall refer to this revised version of Eq. (8) as “modified” Drude weight, $\tilde{D}_{\alpha\beta}$ in the following.] We ascribe this outcome to the well-known ambiguities that arise when combining nlPSPs with electromagnetic fields [40–42]; in practice, we find that its quantitative impact is small.

In Fig. 1 we plot the naBEC Z^* , standard DW D , and modified DW \tilde{D} , for FCC Al versus the number of k -points used to sample the Brillouin zone of the conventional cubic cell [43]. Since FCC Al has no optical modes, the nonadiabatic regime is hardly relevant here from a physical point of view; yet, given its computational simplicity, this is an excellent first numerical test to benchmark our arguments. Remarkably, the naBEC of Al does not vanish in spite of it being an elemental

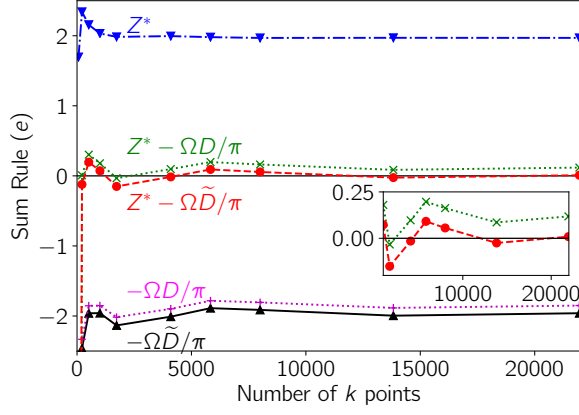


FIG. 1. Demonstration of nonadiabatic Born effective charge (naBEC) sum rule for Al versus k points in the Brillouin zone of the conventional 4-atom cell. Blue dot-dashed curve is the naBEC, which clearly deviates from zero, the black solid curve is minus the cell volume multiplied by the modified DW [see Eq. (6)], and red dashed curve is the sum of the two which vanishes for sufficiently large k mesh.

metal, and converges to a value of around $2e$. We see from the red dashed curve that the sum rule in Eq. (6) is accurately satisfied for a large enough k mesh. We also see that \tilde{D} differs slightly from D , and this results in a violation of the naBEC sum rule that is modest ($\sim 0.1 e$) but clearly discerned for the numerical accuracy of our calculations. We find a similar qualitative behavior for all materials in this study (see, e.g., SM [37] Figs. S7, S8, and S9); thus, we shall exclusively focus on $\tilde{D}_{\alpha\beta}$ henceforth.

We now consider bulk SnS_2 , a layered insulator that has shown considerable promise for use in a wide range of applications including photocatalysis [44, 45], Li-ion batteries [46, 47], solar cells [48], and field-effect transistors [49]. We dope SnS_2 with electrons via a “rigid band approximation,” i.e., all matrix elements and structural parameters are taken from an undoped calculation, and just the occupation factors are changed to reflect the added electrons (we will confirm the accuracy of this approximation in the context of STO below). The excess positive charge to compensate the electrons is added to Z_{κ}^{ion} , corresponding to chemical doping on either the Sn or S sublattice. In order to accurately describe the Fermi surface, we perform the Brillouin-zone integrals of Eqs. (7) and (8) via Wannier interpolation to a dense k mesh (see SM [37] Secs. S2 B and S2 C). Such an approach is facilitated by the favorable electronic band structure of SnS_2 , where the lowest-energy conduction states form a single isolated band with $\text{Sn}(5s)$ - $\text{S}(3p)$ hybrid character (see Fig. S2(b) in the SM [37]).

In Fig. 2(a), we show the naBECs versus doping for the Sn and S sublattices, in the in-plane x and out-of-plane z directions. The dotted curves in Fig. 2(a) correspond to

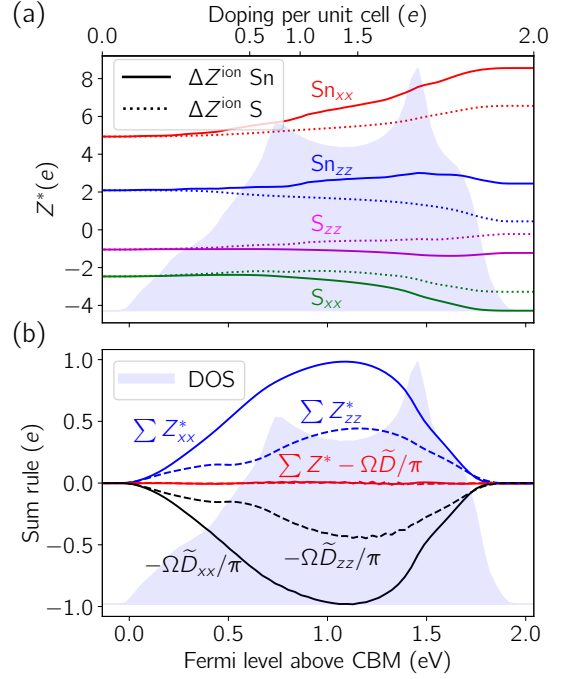


FIG. 2. (a) Nonadiabatic Born effective charges (naBEC) versus doping in the in-plane x direction and out-of-plane z direction. Solid (dotted) lines are for the excess ionic charge ΔZ^{ion} associated with the Sn (S) sublattice. (b) Demonstration of the naBEC sum rule, where the sublattice sum of the BECs equals the Drude weight. Blue shaded region is the DOS of the conduction band calculated from the Wannier interpolation.

the excess ionic charge placed on the S sublattices, and the solid curves to the charge placed on the Sn sublattice. In Fig. 2(b) we see that the violation of the (sublattice-summed) BEC charge neutrality condition increases as we dope to roughly half of the conduction-band width, and then decreases back to zero when the conduction band is filled. The DW exhibits the same behavior, and we see from the red curves around zero, that the naBEC sum rule [Eq. (6)] is accurately satisfied.

Finally we calculate the naBECs and DW for the electron-doped cubic perovskite ($Pm\bar{3}m$) phase of STO. Doped STO has attracted significant attention due to its superconducting properties [50–52], and represents a more complicated conduction band than SnS_2 , formed from $\text{Ti } 3d t_{2g}$ states [53] (See Fig. S2(a) in the SM [37]). We perform the same procedure of rigid-band doping and Wannier interpolation as for SnS_2 .

In Fig. 3(a) we plot the naBECs for the sublattices in STO with doping. For a given BEC element Z_{ii}^* , there are two “equatorial” oxygens on the faces of the cubic cell parallel to \hat{i} , that have equal BECs; the oxygen on the face perpendicular to \hat{i} is labelled as “apical” in Fig. 3(a), and has a larger-magnitude BEC than the equatorial O. Different trends in Z^* result from differ-

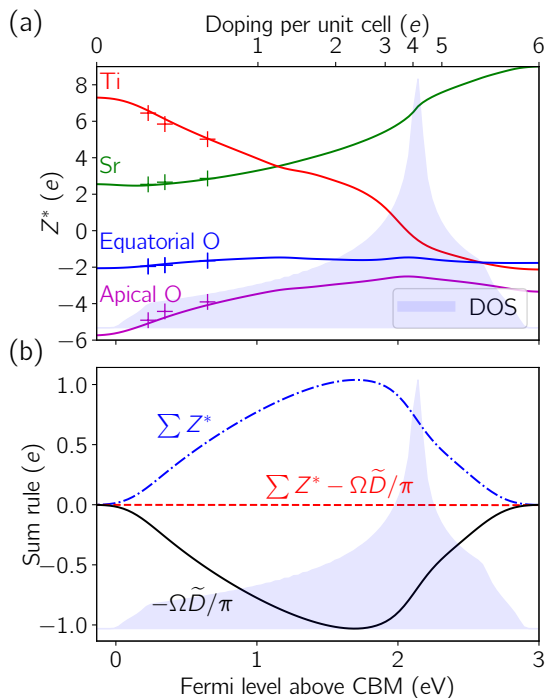


FIG. 3. (a) Nonadiabatic Born effective charges of the sublattices in SrTiO_3 versus doping above the conduction-band minimum (CBM) on the Sr sublattice. The crosses represent virtual-crystal calculations done by mixing the Sr pseudopotential with La. (b) The naBEC sum rule, where the sublattice sum of the BECs cancels with the Drude weight. Blue shaded region superimposed is the density of states of the Wannierized Ti t_{2g} manifold.

ent choices of sublattice for chemical doping (see SM [37] Sec. S3), suggesting significant qualitative changes in frequencies of polar-phonon modes depending on the sublattice that is doped versus the sublattice(s) involved in the phonon displacements. Fig. 3(a) corresponds to doping on the Sr site, e.g., by La substitution; in this case, the Sr Z^* increases significantly to compensate the decrease of the Ti Z^* (which even becomes negative), resulting from the fact that the electrons are doped into the Ti $3d$ orbitals. The crosses in Fig. 3(a) represent calculations done with the same methodology as discussed above, but with the doping explicitly introduced via the virtual-crystal approximation (alchemical mixing of Sr and La pseudopotentials). We see that the results match well with those of the rigid band approximation.

In Fig. 3(b), we plot the DW and sublattice sum of the naBECs. We see very similar behavior to SnS_2 [Fig. 2(b)], where the sum of the BECs increasingly deviates from zero with doping towards the middle of the conduction-band manifold, and then decreases. As with SnS_2 , the naBEC sum rule is accurately satisfied.

In conclusion, we have demonstrated that nonadiabatic Born effective charges are well-defined in metals with time-reversal symmetry, and generalized the acous-

tic sum rule to the full nonadiabatic regime, where the sublattice sum of the nonadiabatic Born effective charges equals the Drude weight. The rigorous understanding and first-principles description of nonadiabatic Born effective charges provided by this work opens up several future directions for study. For example, it will allow quantitative predictions of plasmon-phonon coupling, and the implications for transport in doped semiconductor devices such as transparent conductors. Direct comparison with experimental probes such as infrared or Raman scattering will serve to validate the theory and aid in materials characterization. It may also shed light on the physics of ferroelectric metals, possibly providing additional tools to quantify the amplitude of the polar lattice distortion.

We thank D. Vanderbilt and R. Resta for discussions and insightful comments on the manuscript. CED acknowledges support from the National Science Foundation under Grant No. DMR-1918455. SC acknowledges support from the National Science Foundation under Grant No. DMR-1848074. MS acknowledges support from the European Research Council (ERC) through Grant “MULTIFLEXO” No. 724529; from Ministerio de Economía, Industria y Competitividad (MINECO-Spain) through Grants No. PID2019-108573GB-C22 and No. CEX2019-000917-S; and from Generalitat de Catalunya (Grant No. 2017 SGR1506). The Flatiron Institute is a division of the Simons Foundation.

-
- [1] F. Giustino, *Rev. Mod. Phys.* **89**, 015003 (2017).
 - [2] S. Baroni, S. de Gironcoli, A. Dal Corso, and P. Gianozzi, *Rev. Mod. Phys.* **73**, 515 (2001).
 - [3] M. Born and K. Huang, *Dynamical theory of crystal lattices* (Clarendon press, 1954).
 - [4] R. H. Lyddane, R. G. Sachs, and E. Teller, *Phys. Rev.* **59**, 673 (1941).
 - [5] R. M. Pick, M. H. Cohen, and R. M. Martin, *Phys. Rev. B* **1**, 910 (1970).
 - [6] X. Gonze and C. Lee, *Phys. Rev. B* **55**, 10355 (1997).
 - [7] P. Vogl, *Phys. Rev. B* **13**, 694 (1976).
 - [8] J. Sjakste, N. Vast, M. Calandra, and F. Mauri, *Phys. Rev. B* **92**, 054307 (2015).
 - [9] C. Verdi and F. Giustino, *Phys. Rev. Lett.* **115**, 176401 (2015).
 - [10] R. M. Martin, *Phys. Rev. B* **5**, 1607 (1972).
 - [11] J. Hong and D. Vanderbilt, *Phys. Rev. B* **88**, 174107 (2013).
 - [12] M. Stengel, *Phys. Rev. B* **88**, 174106 (2013).
 - [13] R. Resta, M. Posternak, and A. Baldereschi, *Phys. Rev. Lett.* **70**, 1010 (1993).
 - [14] W. Zhong, R. D. King-Smith, and D. Vanderbilt, *Phys. Rev. Lett.* **72**, 3618 (1994).
 - [15] P. Ghosez, J.-P. Michenaud, and X. Gonze, *Phys. Rev. B* **58**, 6224 (1998).
 - [16] R. Resta, *Rev. Mod. Phys.* **66**, 899 (1994).
 - [17] M. Born and R. Oppenheimer, *Annalen der Physik* **389**,

- 457 (1927).
- [18] G. Petretto, S. Dwaraknath, H. P.C. Miranda, D. Winston, M. Giantomassi, M. J. van Setten, X. Gonze, K. A. Persson, G. Hautier, and G.-M. Rignanese, *Scientific Data* **5**, 180065 (2018).
 - [19] B. B. Varga, *Phys. Rev.* **137**, A1896 (1965).
 - [20] C. G. Olson and D. W. Lynch, *Phys. Rev.* **177**, 1231 (1969).
 - [21] M. Calandra, G. Profeta, and F. Mauri, *Phys. Rev. B* **82**, 165111 (2010).
 - [22] A. M. Saitta, M. Lazzeri, M. Calandra, and F. Mauri, *Phys. Rev. Lett.* **100**, 1 (2008).
 - [23] O. Bistoni, P. Barone, E. Cappelluti, L. Benfatto, and F. Mauri, *2D Materials* **6**, 045015 (2019).
 - [24] L. Binci, P. Barone, and F. Mauri, *arXiv e-prints*, arXiv:2006.02376 (2020).
 - [25] S. Pisana, M. Lazzeri, C. Casiraghi, K. S. Novoselov, A. K. Geim, A. C. Ferrari, and F. Mauri, *Nat. Mater.* **6**, 198 (2007).
 - [26] P. W. Anderson and E. Blount, *Phys. Rev. Lett.* **14**, 217 (1965).
 - [27] Y. Shi, Y. Guo, X. Wang, A. J. Princep, D. Khalyavin, P. Manuel, Y. Michiue, A. Sato, K. Tsuda, S. Yu, *et al.*, *Nat. Mater.* **12**, 1024 (2013).
 - [28] S. L. Adler, *Phys. Rev.* **126**, 413 (1962).
 - [29] P. B. Allen, in *Conceptual Foundations of Materials: A Standard Model for Ground- and Excited-State Properties*, edited by S. G. Louie and M. L. Cohen (Elsevier B.V., Amsterdam, The Netherlands, 1993) Chap. 6, pp. 165–218.
 - [30] R. Resta, *J. Phys. Condens. Mat.* **30**, aade19 (2018).
 - [31] D. J. Thouless, M. Kohmoto, M. P. Nightingale, and M. den Nijs, *Phys. Rev. Lett.* **49**, 405 (1982).
 - [32] X. Gonze, *Phys. Rev. B* **55**, 10337 (1997).
 - [33] M. Stengel, *Nat. Commun.* **4**, 2693 (2013), article.
 - [34] M. Stengel and D. Vanderbilt, *Phys. Rev. B* **98**, 125133 (2018).
 - [35] A. Schiaffino, C. E. Dreyer, D. Vanderbilt, and M. Stengel, *Phys. Rev. B* **99**, 085107 (2019).
 - [36] W. Kohn and L. J. Sham, *Phys. Rev.* **140**, A1133 (1965).
 - [37] See supplemental material [URL to be inserted by publisher] for details of the DFPT formalism, computational approach and convergence, and details about doping of STO.
 - [38] E. Maksimov and S. Shulga, *Solid State Commun.* **97**, 553 (1996).
 - [39] R. van Leeuwen, *Phys. Rev. B* **69**, 115110 (2004).
 - [40] S. Ismail-Beigi, E. K. Chang, and S. G. Louie, *Phys. Rev. Lett.* **87**, 087402 (2001).
 - [41] C. J. Pickard and F. Mauri, *Phys. Rev. Lett.* **91**, 196401 (2003).
 - [42] C. E. Dreyer, M. Stengel, and D. Vanderbilt, *Phys. Rev. B* **98**, 075153 (2018).
 - [43] Note that the cubic symmetry means $Z_{x,\kappa x}^* = Z_{y,\kappa y}^* = Z_{z,\kappa z}^* \equiv Z^*$ and, e.g., $D_{xx} = D_{yy} = D_{zz} \equiv D$.
 - [44] H. Song, S. Li, L. Gao, Y. Xu, K. Ueno, J. Tang, Y. Cheng, and K. Tsukagoshi, *Nanoscale* **5**, 9666 (2013).
 - [45] J. Yu, C.-Y. Xu, F.-X. Ma, S.-P. Hu, Y.-W. Zhang, and L. Zhen, *ACS Appl. Mater. Inter.* **6**, 22370 (2014).
 - [46] J.-w. Seo, J.-t. Jang, S.-w. Park, C. Kim, B. Park, and J. Cheon, *Adv. Mater.* **20**, 4269 (2008).
 - [47] B. Luo, Y. Fang, B. Wang, J. Zhou, H. Song, and L. Zhi, *Energy & Environmental Science* **5**, 5226 (2012).
 - [48] W. Chu, X. Li, S. Li, J. Hou, Q. Jiang, and J. Yang, *ACS Appl. Energy Mater.* **2**, 382 (2018).
 - [49] H. Song, S. Li, L. Gao, Y. Xu, K. Ueno, J. Tang, Y. Cheng, and K. Tsukagoshi, *Nanoscale* **5**, 9666 (2013).
 - [50] J. F. Schooley, W. R. Hosler, E. Ambler, J. H. Becker, M. L. Cohen, and C. S. Koonce, *Phys. Rev. Lett.* **14**, 305 (1965).
 - [51] D. Huang and J. E. Hoffman, *Annu. Rev. Condens. Matt. Phys.* **8**, 311 (2017).
 - [52] C. Collignon, X. Lin, C. W. Rischau, B. Fauqué, and K. Behnia, *Annu. Rev. Condens. Matt. Phys.* **10**, 25 (2019).
 - [53] We present doping across the entire t_{2g} manifold in SrTiO_3 , even though it is not expected to be experimentally achievable, in order to illustrate the behavior of the nonadiabatic Born effective charges. Also, we should note that significant changes to the electronic and atomic structure are expected if such calculations at high doping are performed self-consistently [54].
 - [54] L. Bjaalie, A. Janotti, B. Himmetoglu, and C. G. Van de Walle, *Phys. Rev. B* **90**, 195117 (2014).

Supplemental Material: Nonadiabatic Born effective charges in metals and the Drude weight

Cyrus E. Dreyer,^{1,2} Sinisa Coh,³ and Massimiliano Stengel^{4,5}

¹*Department of Physics and Astronomy, Stony Brook University, Stony Brook, New York, 11794-3800, USA*

²*Center for Computational Quantum Physics, Flatiron Institute,
162 5th Avenue, New York, New York 10010, USA*

³*Materials Science and Mechanical Engineering, University of California Riverside, CA 92521, USA*

⁴*Institut de Ciència de Materials de Barcelona (ICMAB-CSIC), Campus UAB, 08193 Bellaterra, Spain*

⁵*ICREA-Institució Catalana de Recerca i Estudis Avançats, 08010 Barcelona, Spain*

(Dated: December 23, 2024)

S1. DETAILS OF DFPT FORMALISM

We will perform our derivation and ultimately our calculations in the framework of planewave/pseudopotential Kohn-Sham^{S1} DFT. Thus $\psi_{n\mathbf{k}}(\mathbf{r}) = u_{n\mathbf{k}}(\mathbf{r})e^{i\mathbf{k}\cdot\mathbf{r}}$ corresponds to the single-particle wavefunction of band n and wavevector \mathbf{k} in the first Brillouin zone that is the solution of the Kohn-Sham equation with the single particle Hamiltonian

$$\hat{\mathcal{H}} = \hat{T} + \hat{V}_{\text{Hxc}}[\rho] + \hat{V}_{\text{ext}}, \quad (\text{S1})$$

where \hat{T} is the single-particle kinetic energy, $\hat{V}_{\text{Hxc}}[\rho]$ denotes the Hartree and exchange-correlation (Hxc) potential, which is a functional of the density ρ , and \hat{V}_{ext} is the external potential that includes the pseudopotential operators (local and nonlocal). We will often use the “cell-periodic” version of operators: $\hat{\mathcal{O}}_{\mathbf{k}} = e^{-i\mathbf{k}\cdot\mathbf{r}}\hat{\mathcal{O}}e^{i\mathbf{k}\cdot\mathbf{r}}$ which operate on the cell-periodic functions $u_{n\mathbf{k}}(\mathbf{r})$.

A. Generalized susceptibility

We begin with the generalized susceptibility introduced in the main text, and partition it in the following way

$$\chi_{\lambda_1\lambda_2}^{\text{na}}(\omega, \mathbf{q}) = \chi_{\lambda_1\lambda_2}^{\text{geom}}(\mathbf{q}) + \chi_{\lambda_1\lambda_2}^{\text{Kubo}}(\omega, \mathbf{q}). \quad (\text{S2})$$

The “geometric” contribution only depends on the unperturbed density operator, $\hat{\rho}$, and is independent of ω . Taking immediately the limit of $\mathbf{q} \rightarrow 0$,

$$\chi_{\lambda_1\lambda_2}^{\text{geom}} = \text{Tr} \left(\hat{H}_{\mathbf{k}}^{\lambda_1\lambda_2} \hat{\rho} \right), \quad \hat{\rho}_{\mathbf{k}} = \sum_n |u_{n\mathbf{k}}\rangle f_{n\mathbf{k}} \langle u_{n\mathbf{k}}|, \quad (\text{S3})$$

where $\hat{H}_{\mathbf{k}}^{\lambda_1\lambda_2} = \partial^2 \hat{H}_{\mathbf{k}} / \partial \lambda_1 \partial \lambda_2$ is the second derivative of the external potential (i.e., not containing the SCF part), and $f_{n\mathbf{k}}$ is the occupation of band n at k -point \mathbf{k} . Note that the trace implicitly consists of a sum over bands and Brillouin-zone average,

$$\text{Tr} \left(\hat{A} \hat{B} \right) = \int [d^3k] \sum_{mn} \langle u_{m\mathbf{k}} | \hat{A}_{\mathbf{k}} | u_{n\mathbf{k}} \rangle \langle u_{n\mathbf{k}} | \hat{B}_{\mathbf{k}} | u_{m\mathbf{k}} \rangle. \quad (\text{S4})$$

The second term in Eq. (S2) can be written as

$$\chi_{\lambda_1\lambda_2}^{\text{Kubo}}(\omega, \mathbf{q}) = \text{Tr} \left[\hat{H}_{\mathbf{k},\mathbf{q}}^{\lambda_1\dagger} \hat{\rho}^{\lambda_2}(\omega, \mathbf{q}) \right], \quad (\text{S5})$$

where the first-order density matrix is written as a double sum over states

$$\hat{\rho}_{\mathbf{k}}^{\lambda}(\omega, \mathbf{q}) = \lim_{\eta \rightarrow 0} \sum_{nm} \bar{f}_{nm\mathbf{k}}(\omega + i\eta, \mathbf{q}) |u_{m\mathbf{k}+\mathbf{q}}\rangle \langle u_{m\mathbf{k}+\mathbf{q}} | \hat{\mathcal{H}}_{\mathbf{k},\mathbf{q}}^{\lambda}(\omega) | u_{n\mathbf{k}}\rangle \langle u_{n\mathbf{k}}|, \quad (\text{S6})$$

with

$$\bar{f}_{nm\mathbf{k}}(z, \mathbf{q}) = \frac{f_{n\mathbf{k}} - f_{m\mathbf{k}+\mathbf{q}}}{\epsilon_{n\mathbf{k}} - \epsilon_{m\mathbf{k}+\mathbf{q}} + z}. \quad (\text{S7})$$

Note that the first-order Hamiltonian becomes ω -dependent via the charge self-consistency once the local fields are incorporated,

$$\hat{\mathcal{H}}^\lambda(\omega) = \hat{H}^\lambda + \hat{V}_{\text{Hxc}}^\lambda(\omega) \quad (\text{S8})$$

where \hat{H}^λ is the kinetic energy and external potential perturbation, and $\hat{V}_{\text{Hxc}}^\lambda$ is the potential response containing self-consistent fields (SCF) that depends on the first-order density, $\rho_{\mathbf{q}}^\lambda(\mathbf{r}, \omega) = \langle \mathbf{r} | \hat{\rho}^{\lambda_2}(\omega, \mathbf{q}) | \mathbf{r} \rangle$ as

$$\hat{V}_{\text{Hxc}}^\lambda(\mathbf{r}, \omega) = \int d^3r' K_{\text{Hxc}}(\mathbf{r}, \mathbf{r}') \rho^{\lambda, \omega}(\mathbf{r}, \omega), \quad (\text{S9})$$

where K_{Hxc} is the Hxc kernel, defined as the variation of the SCF potential with respect to a charge-density perturbation.

B. Adiabatic regime

If we take $\omega \rightarrow 0$, the intraband contribution in Eq. (S5) remains finite, and

$$\bar{f}_{n\mathbf{k}} \rightarrow \left. \frac{df(\epsilon)}{d\epsilon} \right|_{\epsilon=\epsilon_{n\mathbf{k}}}. \quad (\text{S10})$$

Then, for a $\mathbf{q} = 0$ perturbation, we obtain the *adiabatic* response,

$$\chi_{\lambda_1 \lambda_2}^{\text{ad}} = \text{Tr} \left[\frac{\partial}{\partial \lambda_2} \left(\hat{\rho} \hat{H}^{\lambda_1} \right) \right]. \quad (\text{S11})$$

Note that $\chi_{\lambda_1 \lambda_2}^{\text{ad}}$ is written as a total derivative with respect to one of the perturbations. This means that, if either the λ_1 or λ_2 is a vector potential field, the corresponding perturbation reduces to a partial derivative with respect to k_α , and its BZ average vanishes. Physically, the fact that $\chi_{A_\alpha A_\beta}^{\text{ad}}$ vanishes is a direct consequence of the f -sum rule; the result $\chi_{A_\alpha \tau_{\kappa\beta}}^{\text{ad}} = 0$, on the other hand, tells us that a static atomic displacement cannot produce a steady current. $\chi_{\tau_{\kappa\alpha} \tau_{\kappa'\beta}}^{\text{ad}}$ does not vanish: it is the electronic contribution to the adiabatic force-constant matrix, as it is calculated in most linear-response DFT packages.^{S2-S4}

C. Nonadiabatic response

When considering, e.g., optical phonons in polar crystal lattices, or the response to electromagnetic radiation, it is appropriate to reverse the order of the $\mathbf{q} \rightarrow 0$ and $\omega \rightarrow 0$ limits. The intraband contributions to Eq. (S5) is suppressed in the $\mathbf{q} \rightarrow 0$ limit, thus, we obtain a *nonadiabatic* response function as the *interband* part of the adiabatic one, i.e., by replacing $\hat{\rho}^{\lambda_2}$ in Eq. (S5) with

$$\hat{\rho}_{\mathbf{k}}^{\lambda_2, \text{inter}} = \sum_{n \neq m} \bar{f}_{nm}^{\mathbf{k}} |u_{m\mathbf{k}}\rangle \langle u_{m\mathbf{k}} | \hat{\mathcal{H}}_{\mathbf{k}}^{\lambda_2} |u_{n\mathbf{k}}\rangle \langle u_{n\mathbf{k}}|. \quad (\text{S12})$$

Note that, in principle, the intraband contribution to the first-order charge density should be removed as well, i.e., the adiabatic scattering potential $\hat{\mathcal{H}}^{\lambda_2}$ should be replaced with $\hat{\mathcal{H}}^{\lambda_2, \text{inter}} = \hat{H}^{\lambda_2} + \hat{V}_{\text{Hxc}}^{\lambda_2, \text{inter}}$, and $\hat{V}_{\text{Hxc}}^{\lambda_2, \text{inter}}$ is defined from $\rho^{\lambda_2, \text{inter}}(\mathbf{r})$ via Eq. (S9). While taking this extra step would be desirable, as it would lead to a fully self-consistent computational setup, it would also substantially complicate the implementation; therefore, in our calculations we have retained the adiabatic phonon perturbation, $\hat{\mathcal{H}}^{\lambda_2}$, for simplicity. We believe, in fact, that our calculations are unaffected by such a simplifying assumption, as we shall clarify in the following.

At small (but finite) \mathbf{q} , correctly treating the intraband contribution to the density in the SCF cycles may be important. Whether free carriers participate (full adiabatic density) or do not participate (nonadiabatic interband-only density) to screening a phonon perturbation has obviously a crucial impact on the macroscopic electric fields that are produced, e.g., by a long-wavelength LO mode. Right at the zone center, however, and under the assumption of short-circuit electrical boundary conditions (as required by the definition of the Born dynamical charge tensor), neglecting the nonadiabatic correction to the SCF potential is much safer, since it may only lead to a small discrepancy

in the first-order potential that averages to zero over the cell. Furthermore, in presence of space-inversion symmetry, infrared-active modes (i.e., the only ones carrying a nonzero dynamical charge) do not couple with Fermi-level shifts, and hence their intraband contribution to the density response should vanish. This indicates that our calculations (all performed on centrosymmetric crystals) should not be affected by this issue.

1. Drude weight

Consider the case where both λ_1 and λ_2 are components of the vector potential. The total density response to a translation in \mathbf{k} -space vanishes, so the interband contribution to the density response is minus the intraband one. Also, the density response, and thus the SCF contributions vanish if TRS is present (since $\bar{f}_{nn\mathbf{k}}$ and $|u_{n\mathbf{k}}(\mathbf{r})|^2$ are even under $\mathbf{k} \rightarrow -\mathbf{k}$, while $\langle u_{n\mathbf{k}} | \hat{H}_{\mathbf{k}}^{A\alpha} | u_{n\mathbf{k}} \rangle$ is odd). Thus, the response reduces to the familiar Drude expression (e.g, see Ref. S5),

$$\begin{aligned} \chi_{A_\alpha A_\beta}^{\text{na}} &= - \int [d^3k] \bar{f}_{nn\mathbf{k}} \langle u_{n\mathbf{k}} | \hat{H}_{\mathbf{k}}^{A\alpha} | u_{n\mathbf{k}} \rangle \langle u_{n\mathbf{k}} | \hat{H}_{\mathbf{k}}^{A\beta} | u_{n\mathbf{k}} \rangle \\ &= - \int [d^3k] \bar{f}_{nn\mathbf{k}} \frac{\partial \epsilon_{n\mathbf{k}}}{\partial k_\alpha} \frac{\partial \epsilon_{n\mathbf{k}}}{\partial k_\beta} = \frac{\Omega}{\pi} D_{\alpha\beta}, \end{aligned} \quad (\text{S13})$$

where Ω is the cell volume. $D_{\alpha\beta}$ is the ‘‘Drude weight.’’ This corresponds to the optical conductivity multiplied by $i\omega$. The Drude weight is nonzero in all metals, regardless of crystal symmetry, which is seen by realizing that the square of the Fermi velocities in Eq. (S13) is even under $\mathbf{k} \rightarrow -\mathbf{k}$ even if the crystal has TR and inversion symmetry.

As discussed in the main text, we will also consider a ‘‘modified’’ version of the Drude weight, given by

$$\frac{\Omega}{\pi} \tilde{D}_{\alpha\beta} = - \int [d^3k] \bar{f}_{nn\mathbf{k}} \langle u_{n\mathbf{k}} | \hat{H}_{\mathbf{k}}^{A\alpha} | u_{n\mathbf{k}} \rangle \langle u_{n\mathbf{k}} | \hat{p}_{\beta\mathbf{k}} | u_{n\mathbf{k}} \rangle \quad (\text{S14})$$

where $\hat{p}_{\beta,\mathbf{k}} = -i\nabla_\beta + \hat{k}_\beta$ is the canonical momentum operator.

2. Born effective charges

We will now derive the nonadiabatic response at first order in the velocity, valid for the optical conductivity and the Born effective charges. The derivation rests on the following identity

$$\frac{\Delta f}{\Delta\epsilon + z} = \frac{\Delta f}{\Delta\epsilon} \left(1 - \frac{z}{\Delta\epsilon + z} \right). \quad (\text{S15})$$

The first term in the round brackets does not depend on frequency; summed with the geometric term it yields the adiabatic response, which vanishes both for the current–current and the current–force response functions. From the second term in the round brackets we readily obtain, via Eq. (1) of the main text, the established formula for the optical conductivity (i.e., Eq. (25) of Ref. S6). Similarly, Eq. (2) of the main text yields the electronic contribution to the Born charges as^{S7,S8}

$$Z_{\kappa\beta}^{(\alpha)}(\omega + i\eta) = -\frac{1}{i} \int [d^3k] \sum_{nm} \frac{\bar{f}_{nm\mathbf{k}}}{\epsilon_{n\mathbf{k}} - \epsilon_{m\mathbf{k}} + z} \langle u_{n\mathbf{k}} | \hat{H}_{\mathbf{k}}^{k_\alpha} | u_{m\mathbf{k}} \rangle \langle u_{m\mathbf{k}} | \hat{\mathcal{H}}_{\mathbf{k}}^{\tau_\beta}(z) | u_{n\mathbf{k}} \rangle, \quad (\text{S16})$$

where $\hat{H}_{\mathbf{k}}^{k_\alpha}$ is the velocity operator and $\tau_{\kappa\beta}$ indicates the displacement of the sublattice κ along the Cartesian direction β . After taking the $\omega \rightarrow 0$ limit, we readily obtain the expression for the naBEC given by Eq. (7) of the main text. In an insulator, Eq. (7) reduces to the usual expressions for the adiabatic BEC.

D. Sums over empty states

If we were to calculate the naBEC using Eq. (7) in the main text, then we would have to perform a convergence over empty states. In order to avoid this, we will use the same approach as is common in DFPT, casting the problem in terms of obtaining first-order wavefunctions via solving a Sternheimer equation. To this end, we shall assume that the active subspace of states that are treated explicitly in the calculation spans the lowest M orbitals with occupation

numbers different from zero. Then, we can decompose Eq. (7) in the main text into a double sum over the first M states plus two sums over $1, \dots, M$ and $M+1, \dots$,

$$\begin{aligned} & \lim_{\eta \rightarrow 0^+} \int [d^3k] \sum_{n \leq M, m \leq M} \frac{\bar{f}_{nm\mathbf{k}}}{\epsilon_{n\mathbf{k}} - \epsilon_{m\mathbf{k}} + i\eta} \langle u_{n\mathbf{k}} | \hat{H}_{\mathbf{k}}^{k_\alpha} | u_{m\mathbf{k}} \rangle \langle u_{m\mathbf{k}} | \hat{\mathcal{H}}_{\mathbf{k}}^{\tau_{\kappa\beta}, \text{inter}} | u_{n\mathbf{k}} \rangle \\ & + \int [d^3k] \sum_{n \leq M, m \geq M+1} \frac{f_{n\mathbf{k}}}{(\epsilon_{n\mathbf{k}} - \epsilon_{m\mathbf{k}})^2} \langle u_{n\mathbf{k}} | \hat{H}_{\mathbf{k}}^{k_\alpha} | u_{m\mathbf{k}} \rangle \langle u_{m\mathbf{k}} | \hat{\mathcal{H}}_{\mathbf{k}}^{\tau_{\kappa\beta}, \text{inter}} | u_{n\mathbf{k}} \rangle \\ & - \int [d^3k] \sum_{m \leq M, n \geq M+1} \frac{f_{m\mathbf{k}}}{(\epsilon_{n\mathbf{k}} - \epsilon_{m\mathbf{k}})^2} \langle u_{n\mathbf{k}} | \hat{H}_{\mathbf{k}}^{k_\alpha} | u_{m\mathbf{k}} \rangle \langle u_{m\mathbf{k}} | \hat{\mathcal{H}}_{\mathbf{k}}^{\tau_{\kappa\beta}, \text{inter}} | u_{n\mathbf{k}} \rangle \end{aligned} \quad (\text{S17})$$

The second and third terms can be conveniently rewritten as a Berry curvature in parameter space, so the naBEC can be written as

$$\begin{aligned} Z_{\alpha, \kappa\beta}^* &= Z_{\kappa}^{\text{ion}} \delta_{\alpha\beta} - \text{Im} \left[\int [d^3k] \sum_{n \leq M} f_{n\mathbf{k}} \left(\langle u_{n\mathbf{k}}^{k_\alpha} | u_{n\mathbf{k}}^{\tau_{\kappa\beta}, \text{inter}} \rangle - \langle u_{n\mathbf{k}}^{\tau_{\kappa\beta}, \text{inter}} | u_{n\mathbf{k}}^{k_\alpha} \rangle \right) \right. \\ & \left. + \lim_{\eta \rightarrow 0^+} \int [d^3k] \sum_{n \leq M, m \leq M} \frac{\bar{f}_{nm\mathbf{k}}}{\epsilon_{n\mathbf{k}} - \epsilon_{m\mathbf{k}} + i\eta} \langle u_{n\mathbf{k}} | \hat{H}_{\mathbf{k}}^{k_\alpha} | u_{m\mathbf{k}} \rangle \langle u_{m\mathbf{k}} | \hat{\mathcal{H}}_{\mathbf{k}}^{\tau_{\kappa\beta}, \text{inter}} | u_{n\mathbf{k}} \rangle \right] \end{aligned} \quad (\text{S18})$$

where the first-order wavefunctions are defined via

$$(\hat{\mathcal{H}}_{\mathbf{k}} + a\hat{P}_{\mathbf{k}}^M - \epsilon_{n\mathbf{k}}) | u_{n\mathbf{k}}^\lambda \rangle = -\hat{Q}_{\mathbf{k}}^M \hat{\mathcal{H}}_{\mathbf{k}}^\lambda | u_{n\mathbf{k}} \rangle, \quad (\text{S19})$$

where $\hat{P}_{\mathbf{k}}^M = \sum_n^M | u_{n\mathbf{k}} \rangle \langle u_{n\mathbf{k}} |$ and $\hat{Q}_{\mathbf{k}}^M = 1 - \hat{P}_{\mathbf{k}}^M$ are projectors inside and outside the active space, and a is a constant that needs to be larger than the total bandwidth of the active space. Eq. (S19) has the same form as the Sternheimer equation solved presently in DFPT implementations,^{S2-S4} except that $\hat{P}_{\mathbf{k}}^M$ does not correspond to the ground-state density operator, but instead the projector over an “active space” M , which is chosen to be large enough to encompass all states such that the occupation of the M th band vanishes. We will show in Sec. S1D that the choice of M does not influence the final result.

S2. COMPUTATIONAL APPROACH AND CONVERGENCE

A. Computational parameters

We implemented the methodology for calculating the naBEC and DW in the ABINIT package,^{S9} taking advantage of the DFPT implementation for calculating the (static) response to atomic displacements and infinitesimal electric fields.^{S3,S4} In all cases, η is fixed to be 10^{-5} Ha. Optimized Vanderbilt norm-conserving pseudopotentials^{S10} taken from PSEUDO-DOJO are used for all calculations.

For Al, we use the PBE^{S11} generalized-gradient approximation exchange-correlation functional, as it provides better structural properties compared to LDA (cubic lattice parameter of 7.63 Bohr). We use Fermi-Dirac smearing with a “temperature” of 0.005 Ha. As mentioned in the main text, k -meshes up to $28 \times 28 \times 28$ were used. For the calculation of the naBEC, we used an active space of $M = 40$ bands; we show in Fig. S1 that the total naBEC does not depend on such choice, as long as enough bands are included such that the occupation of the highest band is negligible ($M \geq 20$ for the conventional cubic cell).

For cubic ($Pm\bar{3}m$) SrTiO₃ (STO) and SnS₂, the local density approximation (LDA) functional parametrized in Ref. S12 was used (as they provide better structural properties than GGA for these materials). The relaxed lattice parameter(s) for STO was 7.29 Bohr and for SnS₂ were $a = 6.87$ and $c = 10.78$ Bohr. Gaussian smearing was used with a width of 0.005 Ha, and a “coarse” k -mesh of $8 \times 8 \times 8$ was used for the undoped calculations for STO and 0.001 Ha and $12 \times 12 \times 6$ for SnS₂. (The slightly larger smearing for STO was in order to smooth fluctuations due to the sharp features in the Fermi surface, see Sec. S2C) The linear response quantities necessary for the calculation of the naBEC and DW with electron doping were Wannier interpolated onto a “fine” mesh in k space as discussed in Sec. S2B.

For STO, doping was performed across the entire Ti $3d$ t_{2g} conduction band manifold [see Fig. S2(a)], while for SnS₂, the doping was performed across the single conduction band [see Fig. S2(b)], which has S $3p$ and Sn $5s$ character. As discussed in the main text, electrons were added via the rigid-band approximation, i.e., only the occupation factors

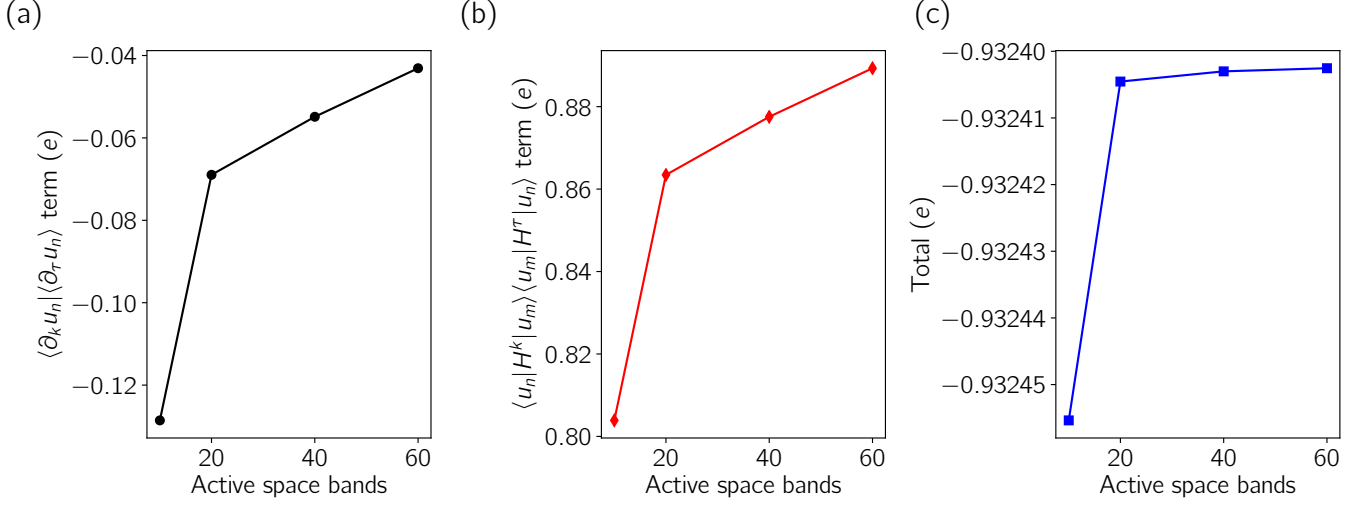


FIG. S1: For cubic cell of FCC Al, the dependence on choice of number of bands in the “active space” M of (a) the second term in Eq. (S18), (b) the third term in Eq. (S18), (c) the total electronic contribution to the nonadiabatic Born effective charge.

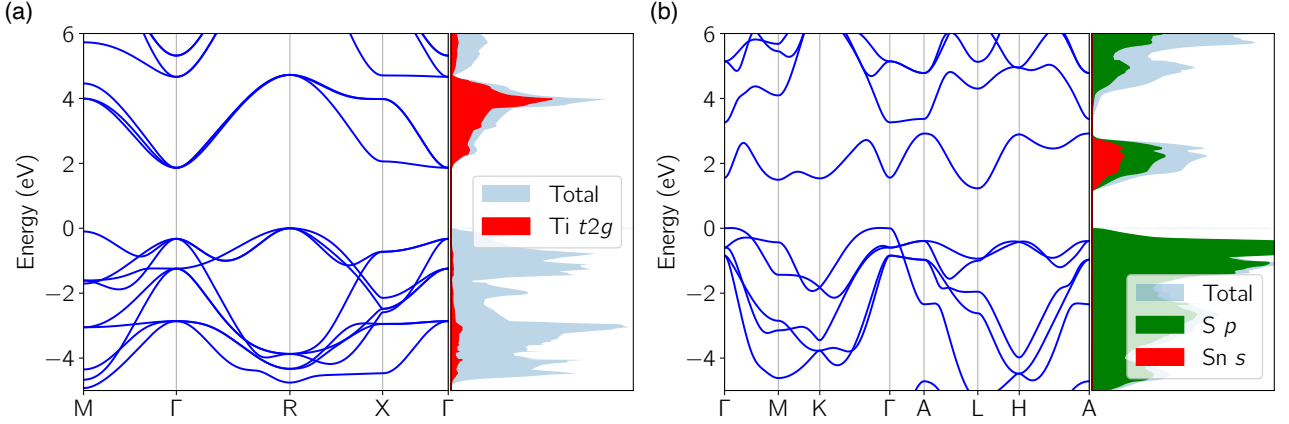


FIG. S2: Bandstructure and projected density of states (DOS) for (a) $Pm\bar{3}m$ SrTiO₃ and (b) SnS₂. Zero energy for each is set to the top of the valence band.

were changed with Fermi level. In Fig. 3(a) in the main text, we compare with explicit doping via the virtual-crystal approximation. To do this, the Sr pseudopotential was alchemically mixed with a La pseudopotential, with all structural properties kept fixed. The same Wannier interpolation procedure (Sec. S2 B) was used in these cases as in the rigid-band calculations. We show in Fig. S3 that such doping does not cause significant qualitative changes to the electronic structure (as long as the structural parameters are fixed).

B. First-order Wannier functions for interpolation

In order to achieve the meshes in k space necessary to converge the naBEC and DW for the doped semiconductors STO and SnS₂, we performed a Wannier interpolation of the quantities in Eqs. (S18), and (S13). Maximally-localized Wannier functions are generated using the WANNIER90^{S13} interface with ABINIT for the valence bands as well as the three lowest-lying conduction bands for STO [Fig. S2(a)], and single lowest-lying conduction band for SnS₂ [Fig. S2(b)]. In order to ensure that a consistent gauge is used, DFPT calculations are initiated from the same ground-state wavefunctions as used for the Wannierization. The unitary transformations that produced the Wannier functions of the ground-state Hamiltonian are used to interpolate the first-order Hamiltonian and wavefunction derivatives (a

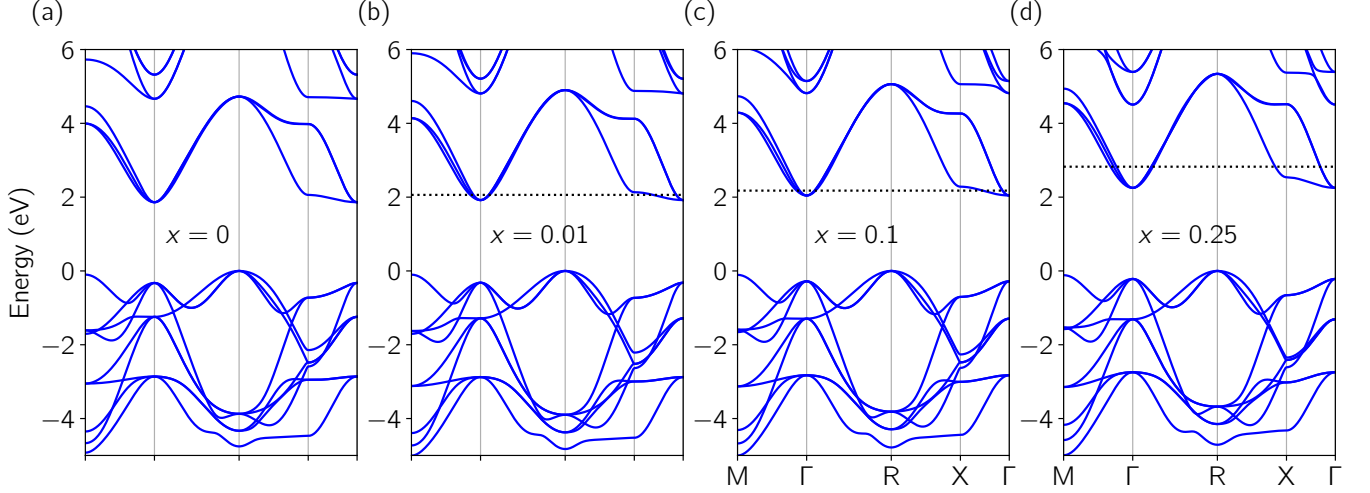


FIG. S3: Band structure using the virtual crystal approximation for $\text{La}_x\text{Sr}_{1-x}\text{TiO}_3$ with various La concentrations. Dotted line is the Fermi level, and energy zero is set to the top of the valence band in all cases.

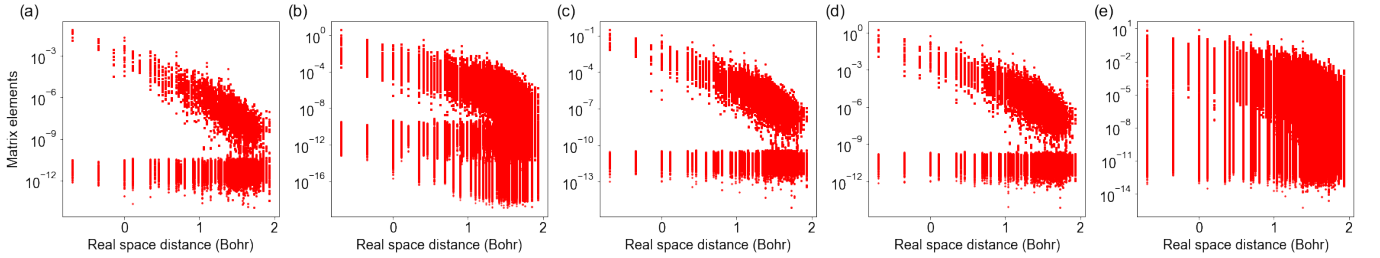


FIG. S4: Decay of the real-space matrix elements of (a) the ground state Hamiltonian, (b) atomic displacement perturbations, (c) velocity operator, (d) momentum operator, and (e), the matrix elements involved in the second term in Eq. (S18).

similar strategy as employed in Ref. S14) onto a fine k -mesh. In order to confirm that this procedure is providing a valid localized basis for interpolation, we plot the decay of the ground state and first-order Hamiltonian matrix elements for STO in real space in Fig. S4 (a similar behavior is observed for SnS_2). For the results in the main text, we use a fine mesh of $100 \times 100 \times 100$ for STO, and $128 \times 128 \times 64$ for SnS_2 .

C. Convergence of nonadiabatic Born effective charges and Drude Weight

In this section we explore the numerical convergence of the naBECs and DW. In Fig. S5 we plot the convergence of the electronic part of the naBECs with interpolated k mesh. We plot separately the second [Fig. S5(a)] and third [Fig. S5(b)] terms in Eq. (S18) (the first ionic term is not included). We can see that the third term, which is nonzero only when empty bands are included in the active space, is the most difficult to converge especially as the van Hove singularity (vHS) is approached. In Fig. S6, we plot the convergence of the naBEC for STO with respect to the width of the Gaussian smearing σ . Similarly to the case with k mesh, the third term in Eq. (S18) shows oscillations for lower meshes as the vHS is approached, that are smoothed with larger smearings. These oscillations could also be removed with larger k meshes.

We turn now to the convergence of Drude weight (DW), and the naBEC sum rule. In the main text, two versions of the DW are discussed, i.e., whether the perturbation and response are both taken to be the *velocity* operators (“velocity-velocity”, which we will denote here as D), or the velocity operator and *momentum* operator (“velocity-momentum”, which we will denote here as \tilde{D}). The velocity and momentum operators differ in our density-functional theory calculations since the pseudopotentials contain nonlocal potentials.^{S15–S18}

In Fig. S7(a) we plot the sublattice sum of the naBEC (including the ionic contribution) for different interpolated k meshes; we see that this sum converges quite rapidly. In Fig. S7(b) and (c) we demonstrate the naBEC sum rule.

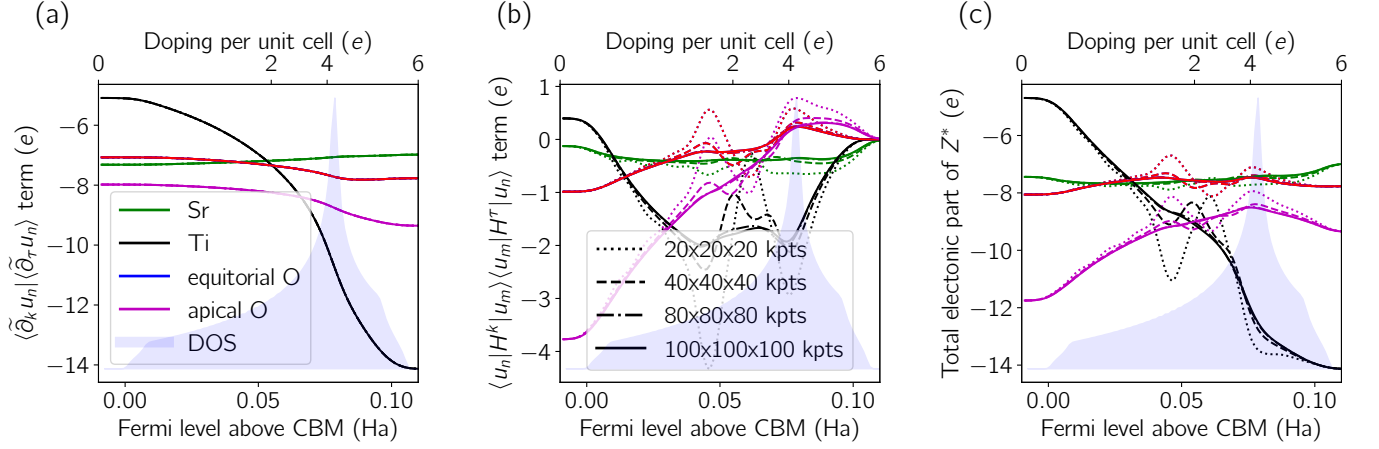


FIG. S5: Convergence of the electronic part of the naBECs of STO with interpolated k mesh. (a) is the second term in Eq. (S18), (b) is the third term in Eq. (S18), and (c) is the total electronic contribution to the nonadiabatic Born effective charge. The density of states of the Ti t_{2g} manifold is superimposed, and the thermal smearing is set to $\sigma = 0.005$ Ha.

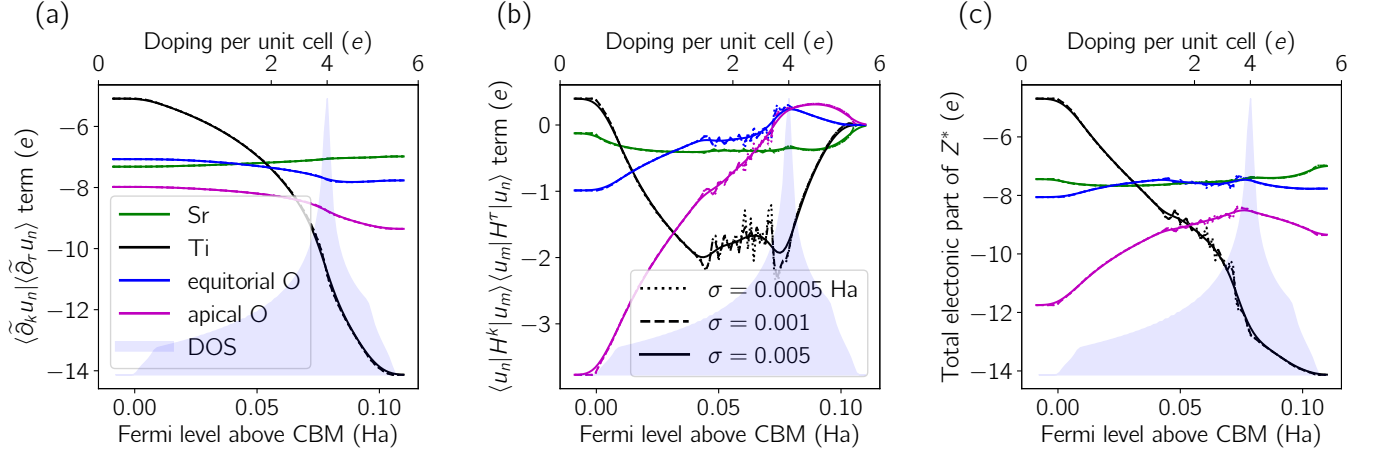


FIG. S6: Same as Fig. S5, demonstrating convergence with respect to thermal smearing, σ (k mesh is fixed to $100 \times 100 \times 100$).

This also converges quickly with k -mesh. Also, we clearly see that the standard DW violates the naBEC sum rule, which is accurately satisfied by the \tilde{D} version. In Fig. S8, we plot the convergence of the same quantities with the smearing. As with the naBECs, we see that a σ of 0.005 Ha is required to smooth the oscillations in the sum rule for a k mesh of $100 \times 100 \times 100$. A larger mesh would allow us to use a smaller smearing.

The convergence behavior is overall quite similar for SnS₂. For example, in Fig. S9 we show the convergence of the naBEC sum rule with interpolated k mesh for both the $\alpha = \beta = \hat{x}$ [Fig. S9(a)-(c)] and $\alpha = \beta = \hat{z}$ [Fig. S9(d)-(f)] components. We see the same behavior as for STO, where the naBEC sum rule is most accurately satisfied for the \tilde{D} version of the DW.

S3. DOPING STO ON DIFFERENT SUBLATTICES

In the main text, we discussed that there is a computational ambiguity for SrTiO₃ as to which sublattice to attribute the extra *ionic* charge ΔZ^{ion} to compensate the electrons added via the rigid band approximation. Physically, this corresponds to chemical doping on different sublattices. In Fig. S10(a), we show the case where the extra charge is attributed to the Sr sublattice, i.e., corresponding to La doping (and compared to doping with La via the virtual crystal approximation). Fig. S10(b) corresponds to doping on the Ti sublattice, e.g., by Nb substitution; here, the

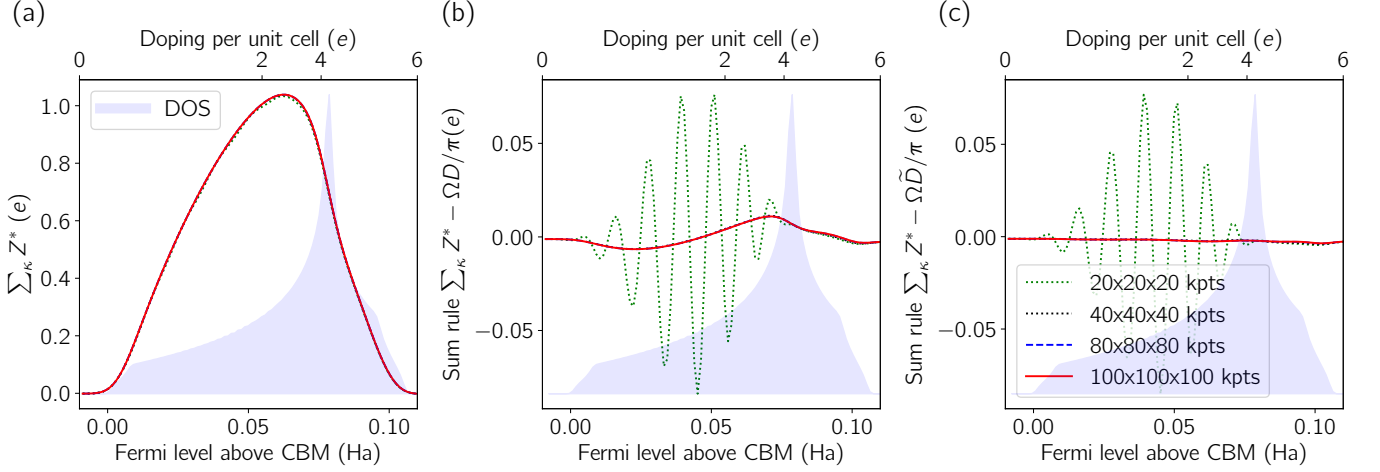


FIG. S7: (a) Sum of nonadiabatic Born effective charges (naBECs), (b) sum of naBECs and standard velocity-velocity Drude weight (DW), (c) sum of naBECs and modified momentum-velocity version of DW, for different k meshes, with the density of states of the Ti t_{2g} manifold superimposed. We set the thermal smearing to $\sigma = 0.005$ Ha

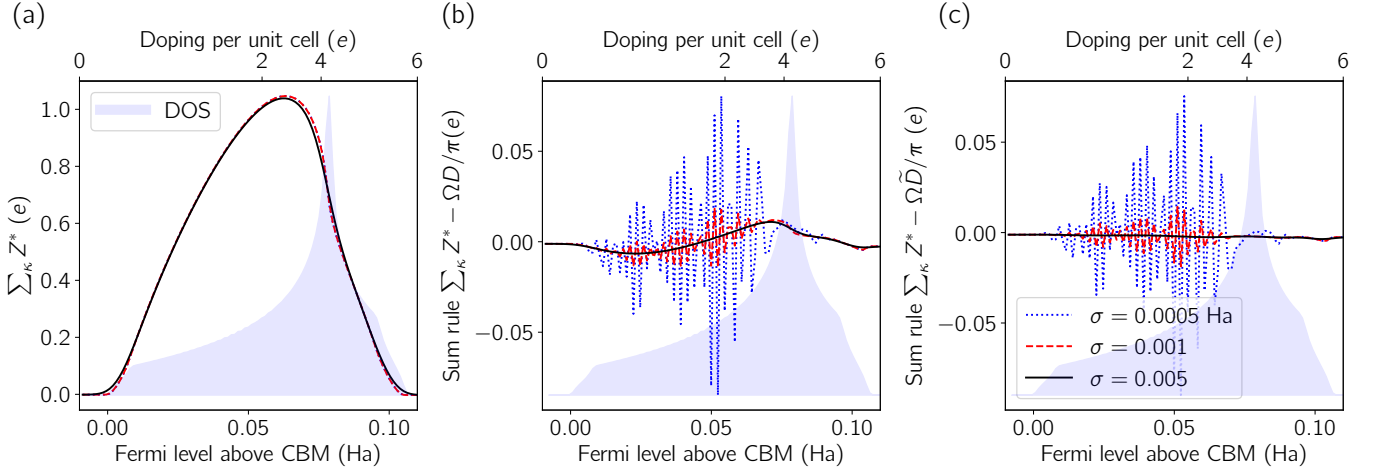


FIG. S8: Same as Fig. S7, but for different values of the thermal smearing σ with the k -mesh set to $100 \times 100 \times 100$.

Ti and Sr Z^* change much less over the doping range, since the electrons and extra ionic charge are on the same site, and thus cancel with each other. Finally, Fig. S10(c) corresponds to doping on the O site, i.e., by the formation of O vacancies; now the O sublattices, especially the apical O (which has the largest hybridization with the Ti $3d$ orbitals^{S19-S21}), increase to compensate the large decrease of the Ti Z^* . This behavior suggests significant qualitative changes in frequencies of polar phonon modes depending on the sublattice that is doped versus the sublattice(s) involved in the phonon displacements.

-
- [S1] W. Kohn and L. J. Sham, Phys. Rev. **140**, A1133 (1965).
[S2] S. Baroni, S. de Gironcoli, A. Dal Corso, and P. Giannozzi, Rev. Mod. Phys. **73**, 515 (2001).
[S3] X. Gonze, Phys. Rev. B **55**, 10337 (1997).
[S4] X. Gonze and C. Lee, Phys. Rev. B **55**, 10355 (1997).
[S5] R. Resta, J. Phys. Condens. Mat. **30**, aade19 (2018).
[S6] P. B. Allen, in *Conceptual Foundations of Materials: A Standard Model for Ground- and Excited-State Properties*, edited by S. G. Louie and M. L. Cohen (Elsevier B.V., Amsterdam, The Netherlands, 1993) Chap. 6, pp. 165–218.
[S7] L. Binci, P. Barone, and F. Mauri, arXiv e-prints, arXiv:2006.02376 (2020).

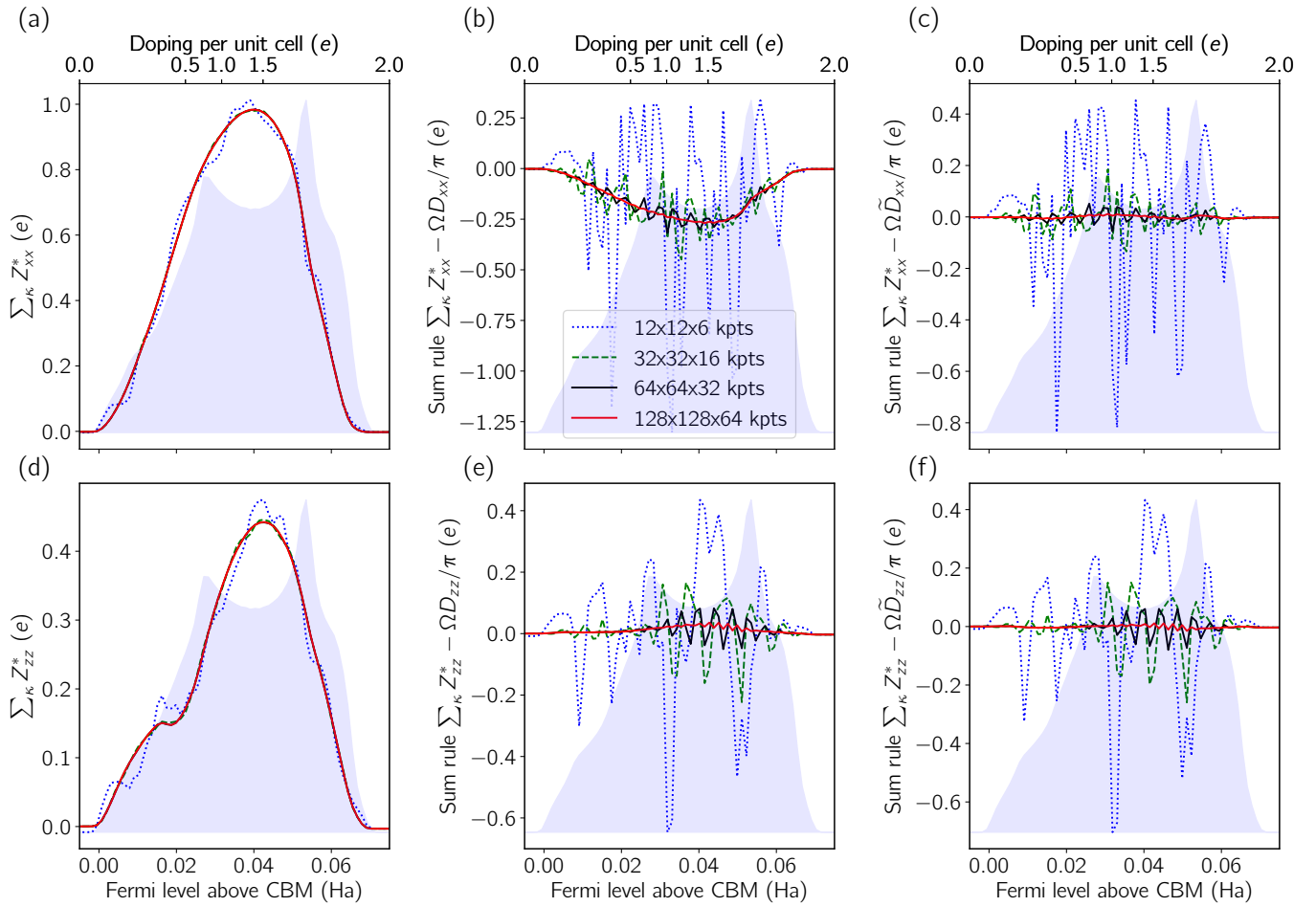


FIG. S9: For SnS₂ using different k meshes, sum of nonadiabatic Born effective charges (naBECs) for the (a) xx and (d) zz components; (b) and (e): sum of naBECs and velocity-velocity Drude weight (DW); (c) and (f): sum of naBECs and momentum-velocity version of DW. The Density of states of the isolated conduction band superimposed. $\sigma = 0.001$ Ha for all calculations.

- [S8] O. Bistoni, P. Barone, E. Cappelluti, L. Benfatto, and F. Mauri, 2D Materials **6**, 045015 (2019).
- [S9] X. Gonze, B. Amadon, P.-M. Anglade, J.-M. Beuken, F. Bottin, P. Boulanger, F. Bruneval, D. Caliste, R. Caracas, M. Côté, T. Deutsch, L. Genovese, P. Ghosez, M. Giantomassi, S. Goedecker, D. Hamann, P. Hermet, F. Jollet, G. Jomard, S. Leroux, M. Mancini, S. Mazevet, M. Oliveira, G. Onida, Y. Pouillon, T. Rangel, G.-M. Rignanese, D. Sangalli, R. Shaltaf, M. Torrent, M. Verstraete, G. Zerah, and J. Zwanziger, Computer Physics Communications **180**, 2582 (2009), 40 {YEARS} {OF} CPC: A celebratory issue focused on quality software for high performance, grid and novel computing architectures.
- [S10] D. R. Hamann, Phys. Rev. B **88**, 085117 (2013).
- [S11] J. P. Perdew, K. Burke, and M. Ernzerhof, Phys. Rev. Lett. **77**, 3865 (1996).
- [S12] J. P. Perdew and Y. Wang, Phys. Rev. B **45**, 13244 (1992).
- [S13] A. A. Mostofi, J. R. Yates, G. Pizzi, Y.-S. Lee, I. Souza, D. Vanderbilt, and N. Marzari, Computer Physics Communications **185**, 2309 (2014).
- [S14] X. Ge and D. Lu, Phys. Rev. B **92**, 241107 (2015).
- [S15] C. E. Dreyer, M. Stengel, and D. Vanderbilt, Phys. Rev. B **98**, 075153 (2018).
- [S16] C. J. Pickard and F. Mauri, Phys. Rev. Lett. **91**, 196401 (2003).
- [S17] S. Ismail-Beigi, E. K. Chang, and S. G. Louie, Phys. Rev. Lett. **87**, 087402 (2001).
- [S18] H. Lu, C.-W. Bark, D. Esque de los Ojos, J. Alcalá, C. B. Eom, G. Catalan, and A. Gruverman, Science **336**, 59 (2012), <http://science.sciencemag.org/content/336/6077/59.full.pdf>.
- [S19] R. Resta, M. Posternak, and A. Baldereschi, Phys. Rev. Lett. **70**, 1010 (1993).
- [S20] W. Zhong, R. D. King-Smith, and D. Vanderbilt, Phys. Rev. Lett. **72**, 3618 (1994).
- [S21] P. Ghosez, J.-P. Michenaud, and X. Gonze, Phys. Rev. B **58**, 6224 (1998).

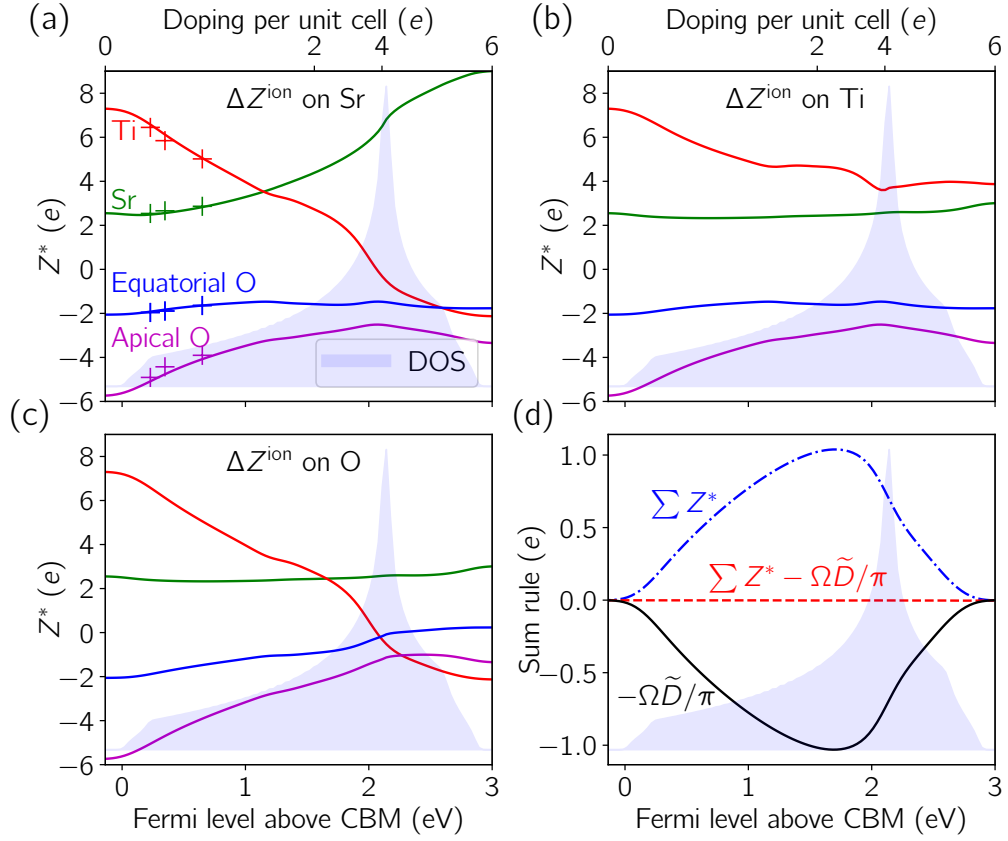


FIG. S10: Nonadiabatic Born effective charges of the sublattices in SrTiO_3 versus doping above the conduction-band minimum (CBM) for doping on (a) the Sr sublattice, (b) the Ti sublattice, and (c) the O sublattice. Pluses in (a) are calculations done with La doping via alchemical mixing of La and Sr pseudopotentials. (d) Demonstrates the naBEC sum rule, where the sublattice sum of the BECs cancels with the Drude weight. Blue shaded region superimposed is the density of states of the Wannierized Ti t_{2g} manifold. Panel (a) and (d) are shown in Fig. 3 in the main text.